

# Test of time dilation by laser spectroscopy on fast ions

**G. Saathoff, S. Reinhardt, H. Buhr, L.A. Carlson, D. Schwalm, A. Wolf, S. Karpuk, C. Novotny, G. Huber, and G. Gwinner**

**Abstract:** The laser-spectroscopic frequency measurement of Doppler-shifted optical lines in the forward and backward directions of a fast ion beam permits a sensitive test of the relativistic Doppler formula and, hence, the relativistic time-dilation factor  $\gamma_{\text{SR}} = 1/\sqrt{1 - v^2/c^2}$ . An experiment on  ${}^7\text{Li}^+$ , stored at a velocity of  $v = 0.065c$  in the Heidelberg heavy-ion storage ring TSR, has confirmed time dilation with unprecedented accuracy limiting deviations to below  $2.2 \times 10^{-7}$ . Ongoing improvements on the experimental setup will further tighten this limit.

PACS Nos.: 03.30.+p, 06.30.Ft, and 42.62.Fi

**Résumé :** La mesure de fréquence par spectroscopie laser des déplacement Doppler des lignes optiques dans les directions avant et arrière d'un faisceau d'ions rapides fournit un test précis de la formule Doppler relativiste et de là, du facteur de dilatation temporelle relativiste  $\gamma_{\text{RS}} = 1/(1 - v^2/c^2)^{1/2}$ . Une expérience avec un faisceau de  ${}^7\text{Li}^+$  de vitesse  $v = 0,065c$ , dans l'anneau de stockage TSR de Heidelberg, a confirmé la dilatation du temps avec une précision sans précédent  $2,2 \times 10^{-7}$ . Les améliorations actuellement apportées au montage devraient améliorer encore cette précision.

[Traduit par la Rédaction]

## 1. Experimental tests of special relativity

Special relativity imposes local Lorentz invariance upon the construction of physical theories. Both quantum field theories in the standard model and general relativity describing gravitation obey this fundamental space-time symmetry. Because of its prominent role, special relativity has been subjected to ever more precise experimental tests. Although no deviation has been found to date, there is still great interest in such experiments, as Lorentz violation has been predicted in attempts to unify the standard model and gravity.

While Einstein derived special relativity (SR) deductively from his two postulates, the relativity principle and the constancy of the speed of light [1], Robertson [2] showed in 1949 that SR can be based on the results of three classical experiments, namely, the Michelson–Morley [3], Kennedy–

Received 5 October 2004. Accepted 28 November 2004. Published on the NRC Research Press Web site at <http://cjp.nrc.ca/> on 13 May 2005.

**G. Saathoff,<sup>1</sup> S. Reinhardt, H. Buhr, L.A. Carlson, D. Schwalm, and A. Wolf.** Max-Planck-Institut für Kernphysik, 69029 Heidelberg, Germany.

**S. Karpuk, C. Novotny, and G. Huber.** Institut für Physik, Universität Mainz, 55099 Mainz, Germany.

**G. Gwinner.** Department of Physics and Astronomy, University of Manitoba, Winnipeg, MB R3T 2N2, Canada.

<sup>1</sup>Corresponding author (e-mail: [guido.saathoff@mpi-hd.mpg.de](mailto:guido.saathoff@mpi-hd.mpg.de)).

Thorndike [4], and the Ives–Stilwell [5] experiments. Possible deviations from SR would occur, if a preferred reference frame  $\Sigma$  exists in the sense that it causes physical effects depending on the velocity relative to this preferred frame. This would constitute an experimental falsification of the relativity principle. The discovery of the cosmic microwave background (CMB) [6] shows that, cosmologically, a preferred reference frame exists, namely, the system in which the CMB appears isotropic. Earth is moving with a velocity of  $V \approx 350$  km/s with respect to the CMB frame. It is customary to quote the sensitivity of the classical SR tests based on the assumption that this reference frame is the preferred frame.

To quantify deviations from the relativity principle, Robertson developed a kinematical test theory [2], that was later modified by Mansouri and Sexl [7]. They consider generalized Lorentz transformations between a hypothetical preferred frame  $\Sigma(T, X)$  and a frame  $S(t, x)$  moving relative to  $\Sigma$  at a velocity  $V$  along the  $X$  axis, and the speed of light is assumed to be isotropic in  $\Sigma$  only. Using Einstein synchronization, these transformations read

$$\begin{aligned} T &= \Gamma \left( \frac{t}{\hat{a}} + \frac{Vx}{\hat{b}c_0^2} \right) \\ X &= \Gamma \left( \frac{x}{\hat{b}} + \frac{Vt}{\hat{a}} \right), \quad Y = \frac{y}{\hat{d}}, \quad Z = \frac{z}{\hat{d}} \end{aligned} \quad (1)$$

with  $\Gamma = (1 - V^2/c_0^2)^{-1/2}$  and  $c_0$  being the speed of light in  $\Sigma$ . Note that due to the abolition of the relativity principle these transformations are, in general, not valid between two arbitrary, constantly moving reference frames but only with respect to  $\Sigma$ . This model contains three velocity-dependent test functions  $\hat{a}(V^2)$ ,  $\hat{b}(V^2)$ , and  $\hat{d}(V^2)$ , which modify time dilation as well as Lorentz contraction in longitudinal and transverse direction. They reduce to  $\hat{a}(V^2) = \hat{b}(V^2) = \hat{d}(V^2) = 1$  in the case SR holds. In the low-velocity limit, these functions can be expanded in powers of  $V^2/c_0^2$ , i.e.,  $\hat{a}(V^2) = [1 + \hat{\alpha}V^2/c_0^2 + \mathcal{O}(c_0^{-4})]$ ,  $\hat{b}(V^2) = [1 + \hat{\beta}V^2/c_0^2 + \mathcal{O}(c_0^{-4})]$ , and  $\hat{d}(V^2) = [1 + \hat{\delta}V^2/c_0^2 + \mathcal{O}(c_0^{-4})]$ . In this regime one is, therefore, left with three test parameters  $\hat{\alpha}$ ,  $\hat{\beta}$ , and  $\hat{\delta}$ .

In this framework, the speed of light  $c(\theta, V)$  in the moving frame  $S$ ,

$$\frac{c(\theta, V)}{c_0} = 1 + (\hat{\beta} - \hat{\delta}) \frac{V^2}{c_0} \sin^2(\theta) + (\hat{\alpha} - \hat{\beta}) \frac{V^2}{c_0} \quad (2)$$

is in general not constant, but is dependent on the angle  $\theta$  between the direction of  $c(\theta, V)$  and the motion of the moving frame  $S$  as well as on the velocity  $V$  between  $\Sigma$  and  $S$ . The Michelson–Morley experiment is sensitive to an anisotropy of the speed of light, thus determining the parameter combination  $|\hat{\beta} - \hat{\delta}|$  and the Kennedy–Thorndike tests the velocity-dependence of  $c$  described by  $|\hat{\alpha} - \hat{\beta}|$ . The Ives–Stilwell experiment independently measures the parameter  $\hat{\alpha}$  that describes time dilation.

No deviation from SR has been found to date in either of the three experiments. The most sensitive interferometric experiments [8, 9] have yielded limits of  $|\hat{\beta} - \hat{\delta}| < 1.5 \times 10^{-9}$  for an anisotropy and of  $|\hat{\alpha} - \hat{\beta}| < 6.9 \times 10^{-7}$  for a velocity-dependence of  $c$ . The best limit on deviations from time dilation prior to the storage ring experiment presented in this paper was  $|\hat{\alpha}| < 1.4 \times 10^{-6}$  [10].

## 2. Principle of the Ives–Stilwell experiment

In Ives–Stilwell-type experiments time dilation is measured via the relativistic Doppler shift of optical lines in moving atoms or ions

$$\nu_0 = \gamma (1 - \beta \cos \vartheta) \nu \quad (3)$$

$\nu_0$  and  $\nu$  denote the transition frequencies in the ions' rest frame and the laboratory frame, respectively,  $\beta = v/c_0$  is the velocity of the source, and  $\vartheta$  the angle between  $\beta$  and the direction of observation in the

laboratory frame. The ions are used as moving clocks and their frequency is measured in the laboratory frame.

In 1907, Einstein proposed to measure time dilation by observing the emitted light of moving particles in the transverse direction, as for  $\vartheta = \pi/2$ , the first-order Doppler effect vanishes and only the purely relativistic contribution stemming entirely from time dilation remains. This approach has been realized in Mößbauer rotor experiments, where the search for the frequency shift between a gamma-ray source and a resonant absorber attached to opposite tips of a high-speed rotor has been undertaken [11]. However, at  $\vartheta = \pi/2$ , (3) is most sensitive to angular misalignment, as the dependence on small deviations from perfect orthogonality is linear. In contrast, at  $\vartheta = 0$  and  $\vartheta = \pi$ , small angular misalignments enter only quadratically. For this reason, the collinear geometry is preferable in experiments using particle beams, where the direction of observation is more difficult to control. To eliminate the first-order Doppler effect present in these collinear experiments, both the parallel and the antiparallel shifts have to be measured simultaneously. This geometry was chosen by Ives and Stilwell [5] in 1938 allowing for the first observation of time dilation, which was at the same time the first observed positive effect of SR. They used excited hydrogen atoms in canal rays moving at  $\beta = 0.005$  and measured the Doppler-shifted frequencies of the  $n = 4 \rightarrow n = 2$  transition in the forward and backward directions using a grating spectrometer.

Within SR, the observed frequencies in parallel ( $\vartheta_p = 0$ ) and antiparallel ( $\vartheta_a = \pi$ ) direction with respect to  $\beta$  are given by

$$\nu_0 = \gamma_{\text{SR}} (1 - \beta \cos \vartheta_{p,a}) \nu_{p,a} \quad (4)$$

Assuming SR to be valid, the multiplication of these two equations yields the velocity-independent relation

$$\nu_0^2 = \nu_a \nu_p \quad (5)$$

since the relativistic time-dilation factor obeys  $\gamma_{\text{SR}}^2 (\beta^2) \times (1 - \beta^2) = 1$ . Within the Mansouri–Sexl test theory, a nonvanishing test parameter  $\hat{\alpha}$  would modify the outcome of the experiment as [12]

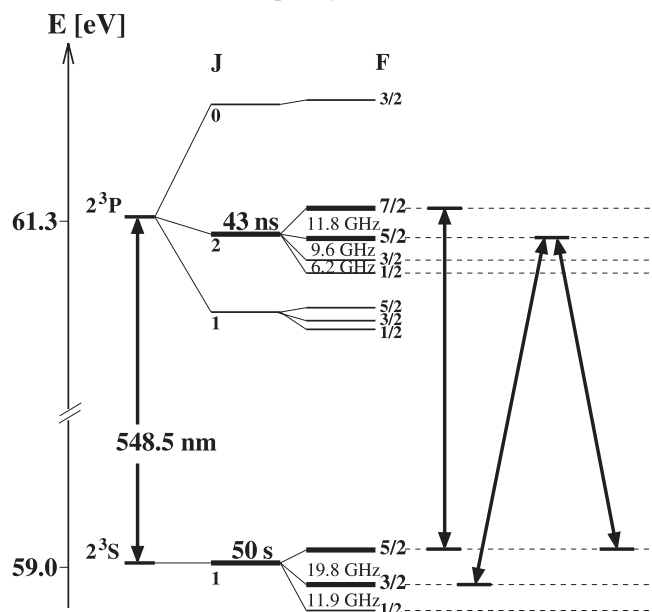
$$\frac{\nu_p \nu_a}{\nu_0^2} = 1 + 2\hat{\alpha} (\beta^2 + 2\beta_{\text{lab}} \cdot \beta) + \mathcal{O}(c_0^{-4}) \quad (6)$$

where  $\beta_{\text{lab}} = \mathbf{V}_{\text{lab}}/c_0$  is the velocity of the laboratory frame with respect to the preferred frame  $\Sigma$ . Note that the result is independent of the synchronization procedure as well as on the test parameters  $\hat{\beta}$  and  $\hat{\delta}$ ; moreover, the  $\beta^2$  term allows for the determination of  $\hat{\alpha}$  absolutely without having to rely on the precise knowledge of  $\beta_{\text{lab}}$  (at least as long as  $\beta$  is larger than  $\beta_{\text{lab}}$ ), while the  $2\beta_{\text{lab}}\beta$  term gives access to  $\hat{\alpha}$  via sidereal modulations. The original Ives–Stilwell experiment provided an absolute upper bound of  $|\hat{\alpha}| < 1 \times 10^{-2}$ . Later, significant improvements were achieved using laser techniques instead of conventional spectrometers; two-photon spectroscopy on a  $\beta = 0.0036$  neon atomic beam set an absolute bound of  $|\hat{\alpha}| < 2.3 \times 10^{-6}$  [13], and, considering the CMB frame as the preferred one ( $\beta_{\text{lab}}c \approx 350$  km/s), even  $|\hat{\alpha}| < 1.4 \times 10^{-6}$  [10] from the limit on sidereal variations.

### 3. The Heidelberg storage-ring experiment

Today, heavy-ion storage rings equipped with electron coolers like the TSR in Heidelberg [14] provide low-divergence ion beams at high velocities. The combination of these fast-ion-beam techniques with high-resolution laser spectroscopy allows for a significant further improvement of the time-dilation measurement. The present experiment uses  ${}^7\text{Li}^+$  ions stored in the TSR at a velocity of  $\beta = 0.065$  (13.3 MeV). The triplet spectrum of the heliumlike  ${}^7\text{Li}^+$  (Fig. 1) has a strong optical transition  $2s\,{}^3S_1 \rightarrow 2p\,{}^3P_2$  at 548.5 nm with a well-resolved and precisely known fine- and hyperfine-structure multiplet. A first version of this experiment that employed collinear optical–optical double-resonance spectroscopy

Fig. 1. Level-scheme of the ortho-heliumlike triplet system of  ${}^7\text{Li}^+$ .

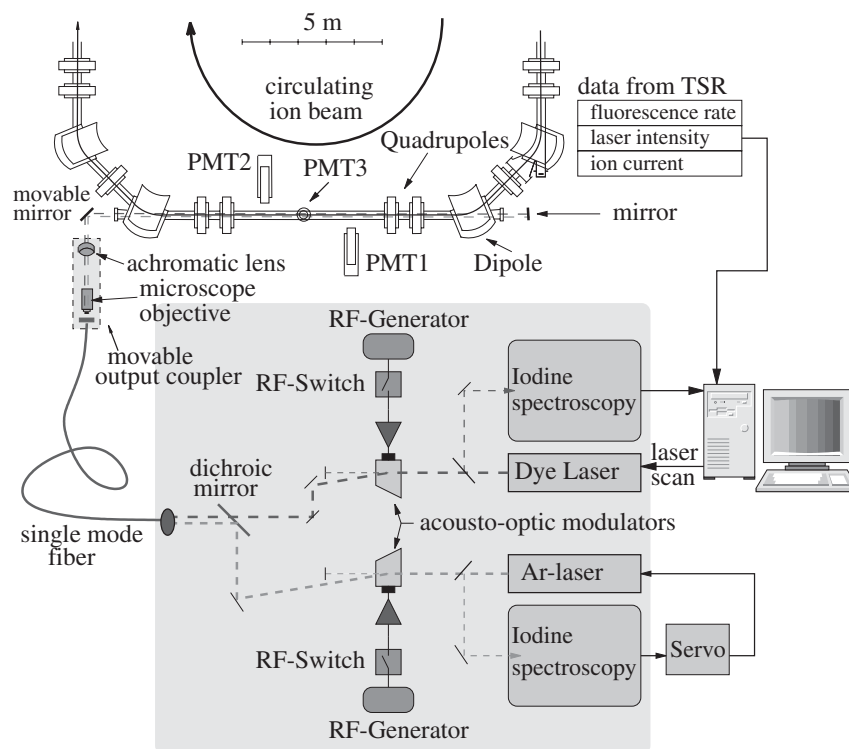


on a  $\Lambda$ -type three-level system formed by the  $2^3S_1(F = 3/2)$ ,  $2^3S_1(F = 5/2)$ , and  $2^3P_2(F = 5/2)$  states has set the hitherto best absolute bound of  $|\hat{\alpha}| < 8 \times 10^{-7}$  [15]. The result was limited by the large observed linewidth of the  $\Lambda$  resonance of almost 60 MHz, compared to a natural width of 3.8 MHz. Time-resolved studies of the  $\Lambda$  system during the present experiment have revealed that most of this broadening was caused by velocity changes between subsequent excitations of the two transitions of the  $\Lambda$  system. The underlying reason is that  $\Lambda$  spectroscopy does not require a *simultaneous* interaction of both lasers with an ion.

This problem is avoided by the application of saturation spectroscopy, which is currently performed on the  $2^3S_1(F = 5/2) \rightarrow 2^3P_2(F = 7/2)$  two-level transition of  ${}^7\text{Li}^+$  at TSR. The laboratory frequencies  $\nu_p$  and  $\nu_a$  of a parallel overlapped fixed-frequency laser and an antiparallel overlapped tunable laser are measured at exact resonance, which is indicated by a Lamb-dip in the fluorescence spectrum. In contrast to the  $\Lambda$ -type measurement, saturation spectroscopy requires the interaction of both lasers with an individual ion within the time-scale of the spontaneous decay of the excited state, which is 43 ns. Velocity-changing processes occur on longer time scales and, hence, do not influence the width of the Lamb dip.

The ion beam is provided by a tandem Van de Graaff accelerator, which starts from negative Li ions and accelerates them towards the positively charged terminal. Here, the ions are gas-stripped to  $\text{Li}^+$  and further accelerated to 13.3 MeV. Typically,  $10^8$  ions are injected into the TSR and kept on a closed orbit of 55.4 m circumference. About 10% of the ions emerge in the metastable  ${}^3S_1$  state from the stripping process. While the lifetime of the metastable ions is 50 s, collisions with the rest gas reduce the beam lifetime to about 13 s. After injection, the ion beam is subjected to electron cooling. At equilibrium, which is reached after about 5 s of cooling, the ion beam has a  $\sigma$ -width of  $\approx 250 \mu\text{m}$ , a  $\sigma$ -divergence of  $\approx 50 \mu\text{rad}$  in the ion-laser interaction region (see Fig. 2), and a longitudinal momentum spread of  $\sigma_p/p = 3.5 \times 10^{-5}$ . The latter leads to a Doppler width of the transition of about 2.5 GHz (FWHM), which is much smaller than the hyperfine splittings (hfs) of the levels involved.

To stabilize the ion velocity, the ion beam is moderately bunched with the third harmonic of the average revolution frequency. Controlling the bunching frequency allows the mean ion velocity to be fine-adjusted and held such that the two-level transition is tuned into resonance with the co-propagating

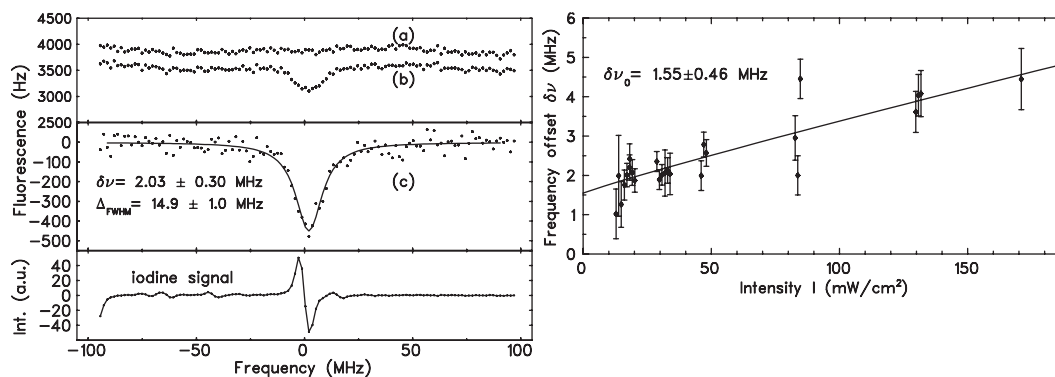
**Fig. 2.** Setup of the experiment at the ion storage ring TSR (from ref. 16).

$\text{Ar}^+$  laser beam at  $\lambda_p = 514.7$  nm exactly for ions in the center of the velocity distribution. The corresponding resonance wavelength of the counterpropagating light is  $\lambda_p = 584.7$  nm, provided by a single-mode dye laser. The frequency measurement of both lasers is accomplished by saturation spectroscopy of hfs lines in molecular iodine, which are calibrated with respect to the primary frequency standard of the Cs atomic clock.

Both laser beams going into the TSR are passed through acousto-optic frequency shifters to switch the light on and off using fast radio-frequency switches. This allows for the subtraction of the Doppler background as described below. The beams are then merged with a dichroic mirror and guided to the TSR by a single-mode polarization-maintaining fiber. At the TSR, the laser beams are linearly polarized in the same direction and their intensities are kept equal to balance the laser forces on the ions. The bichromatic beam coming out of the fiber is directed via an achromatic telescope through the experimental section of the TSR and retro-reflected by a flat mirror. The laser beams are accurately overlapped with the ion beam with computer-controlled motorized translation and (or) rotation stages. By simultaneously maximizing the fluorescence yield recorded with three photomultipliers located at different positions along the beam pipe, the dye laser beam and the ion beam can be aligned to better than  $70 \mu\text{rad}$ .

After each injection, the lasers are switched off for the first 5 s until the ion beam is electron-cooled to equilibrium. Then, the lasers are turned on and the fluorescence rate is recorded as a function of the dye-laser frequency. Figure 3 (left panel) shows a run reflecting 82 laser scans, each spanning 200 MHz in steps of 1 MHz. As the limited lifetime of the metastable ions in the TSR leads to a decrease of the fluorescence background during a laser scan, the laser scan cycles, each consisting of 200 laser steps of 100 ms, are decoupled from the ion injection cycles by injecting a new beam after 46 consecutive laser steps; after adding up a sufficiently large number of scans, the ion-beam decay thus averages out. To remove distortions of the fluorescence signal caused by laser power fluctuations and varying ion currents the Doppler background is measured quasi-simultaneously with the Lamb dip. This is achieved

**Fig. 3.** Left panel: Fluorescence signal observed with PMT3 for a multiple scan of the Lamb dip. Spectrum (a) is plotted with an offset for clarity. The zero of the frequency scale corresponds to the position of the iodine reference line. Right panel: Frequency offset of the Lamb dip from the  $I_2$  reference line as a function of the total laser intensity. The laser switching frequency is 5 kHz (from ref. 16).



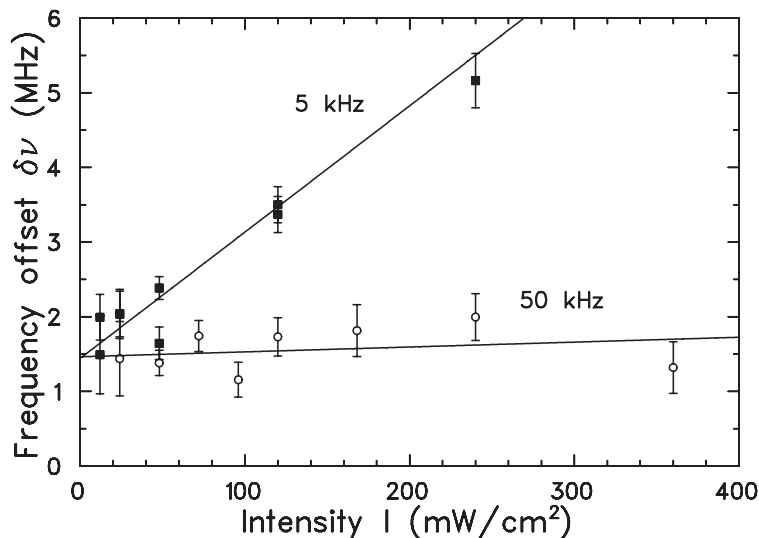
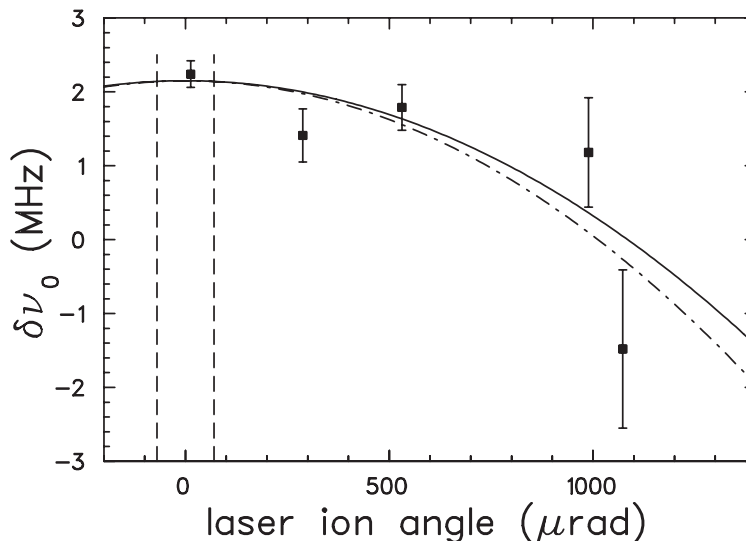
by fast switching between three different laser beam configurations and recording the fluorescence rate into three corresponding separate spectra. One, taken with both lasers interacting with the ions simultaneously, contains the Doppler background together with the Lamb dip (curve (b) in Fig. 3). The other two spectra are recorded with the lasers applied separately, the sum of which reflects the Doppler background alone (curve (a)). Subtracting (a) from (b) leads to the pure Lamb-dip spectrum (c). To record the three fluorescence rates quasi-simultaneously, the acousto-optic modulators are switched at 5 kHz.

### 3.1. Systematics

Several systematic errors have to be taken into account. To prevent a frequency shift due to magnetic stray fields in the experimental section, we apply linearly polarized light. In this case, optical pumping together with the Zeeman effect is expected to cause only a slight broadening but not a net shift of the resonance. In the following, investigations of the influence of laser forces, angular misalignments, and of the Gaussian phase structure of the laser beams on the Lamb-dip frequency are discussed.

#### 3.1.1. Influence of the laser forces

In Fig. 3 (right panel), the Lamb-dip center frequency  $\delta\nu$  is plotted versus the sum of the two laser intensities, which is varied over one order of magnitude. The measurement reveals a slight dependence of about 3 MHz over the whole intensity range, which we attribute to local changes in the velocity distribution caused by the laser forces. These changes modify the Doppler background and lead to distortions of the Lamb dip. Only those distortions that build up on a slower time scale than the laser switching time of 200  $\mu$ s are cancelled out in our background subtraction scheme. To account of the residual effect, we extrapolate the resonance frequency to zero intensity by fitting  $\delta\nu = \delta\nu_L + mI^\kappa$  with  $m$ ,  $\kappa$ , and  $\delta\nu_L$  as fit parameters, yielding an almost linear dependence ( $\kappa = 0.93$ ) with a frequency offset at intensity zero of  $\delta\nu_L = 1550 \pm 460$  kHz relative to the iodine line. Recently, we largely eliminated this intensity dependence by increasing the switching frequency. Figure 4 shows that at a switching frequency of 50 kHz, the Lamb dip is largely independent of the laser intensity, indicating that no significant changes of the velocity distribution occur within 20  $\mu$ s. A linear as well as a constant fit to the data yield essentially the same result and the fit uncertainty is improved to the 100 kHz range. Moreover, the extrapolated Lamb-dip frequencies from measurements taken at 50 kHz and those taken at 5 kHz coincide well within the uncertainty and confirm the fit result in Fig. 3.

**Fig. 4.** Dependence of the Lamb-dip frequency on the laser power at different laser switching frequencies.**Fig. 5.** Measurement of the frequency shift caused by angular misalignment of the two aligned laser beams with respect to the ion beam. The total laser intensity was kept constant at 50 mW/cm<sup>2</sup>.

### 3.1.2. Angular misalignment and laser curvature effects

Deviations of the laser-ion angles  $\vartheta_p$  and  $\vartheta_a$  from 0 and  $\pi$  cause frequency shifts. Assuming plane-wave light, we find  $\Delta\nu_a/\nu_a = -\beta\vartheta_p^2/2(1-\beta)$  in the case of one misaligned laser ( $\vartheta_a = \pi$ ,  $\vartheta_p \neq 0$ , case I), and  $\Delta\nu_a/\nu_a = -\vartheta_p^2\beta^2$  for both lasers mutually aligned, but tilted against the ion beam ( $\vartheta_p = \pi - \vartheta_a \neq 0$ , case II). Figure 5 shows a measurement of the Lamb-dip frequency for different angles between the ion beam and the laser beams (case II). The fit (continuous line) confirms the expectation (dotted-broken line) very well. The vertical broken lines indicate the alignment uncertainty of 70  $\mu\text{rad}$  achieved with the laser-ion overlap procedure described before, which leads to a frequency shift of below 10 kHz. The misalignment of the retro-reflected Ar laser (case I) can also be limited to 70  $\mu\text{rad}$  causing a frequency shift of below 40 kHz.

**Table 1.** Accuracy budget of the saturation spectroscopy; errors are quoted as  $1\sigma$ , all values in kHz.

	Result by Saathoff et al. [16]		Next generation	
	$\beta = 0.06$		$\beta = 0.06$	$\beta = 0.03$
	Frequency	$1\sigma$ error	Error estimates	
Iodine reference line dye	512 671 028 023	152	100	100
Frequency calibration		50	50	100
AOM shift (dye laser) $\delta\nu_{\text{Dye}}^{\text{AOM}}$	414 000	negl.	negl.	negl.
Lamb-dip offset to reference $\delta\nu_{\text{L}}$	1 550	460	150	150
Wave-front corr. (dye laser) $\delta\nu_{\text{Dye}}^{\text{wf}}$	-665	160	70	35
Laser-laser angle		40	40	20
Laser-ion angle		10	10	5
Ion-beam divergence		10	10	5
Total $\nu_{\text{a}}^{\text{exp}}$	512 671 442 908	517	204	210
$\nu_{\text{p}}^{\text{exp}}$ (incl Laser curvature effect)	582 490 203 442	93	99	122
$^7\text{Li}^+$ rest frequency $\nu_0$ [17]	546 466 918 790	400	100	100
SR prediction $\nu_{\text{a}}^{\text{SR}} = \nu_0^2/\nu_{\text{p}}^{\text{exp}}$	512 671 443 186	755	200	
$\nu_{\text{a}}^{\text{exp}} - \nu_{\text{a}}^{\text{SR}}$	-278	915	300	

The divergence of the ion beam leads to small laser-ion angles as well. The influence of the divergence was modeled assuming a monoenergetic ion beam with a Gaussian-angle distribution as well as plane laser waves. Because of the angle with respect to the direction of propagation of the plane laser waves, each ion of the ensemble considered contributes a Lorentzian shifted to lower frequencies. The Lorentzians for all ions are summed up leading to an asymmetric resonance. The corresponding frequency shift for an electron-cooled beam with a divergence of  $50 \mu\text{rad}$  amounts to less than 10 kHz.

A further influence can be caused by the Gaussian phase structure of the laser beams, which shows a phase deviation (Gouy phase shift)  $\xi(z) = \arctan z/z_{\text{R}}$  from a plane wave in direction of the optical axis  $z$ , where  $z_{\text{R}}$  denotes the Rayleigh range and  $z = 0$  the focal point. For a particle travelling along  $z$  with velocity  $v$ , this phase change results in a frequency shift of  $\delta\nu^{\text{wf}} = v d\xi(z)/dz$ . From the measured position of the foci and the Rayleigh ranges of both lasers during the beam time presented here, the shifts are estimated by a Monte Carlo simulation as  $\delta\nu_{\text{a}}^{\text{wf}} = (-665 \pm 160)$  kHz for the dye laser and  $\delta\nu_{\text{p}}^{\text{wf}} = (179 \pm 70)$  kHz for the  $\text{Ar}^+$  laser.

### 3.1.3. Result of the TSR experiment

Taking all systematic errors into account (see Table 1), we find a difference between the dye-laser frequency at the center of the Lamb dip and the value predicted by SR,  $\Delta = \nu_{\text{a}}^{\text{expt}} - \nu_{\text{a}}^{\text{SR}} = -278 \pm 915$  kHz [16]. This is compatible with zero within the  $1\sigma$  uncertainty and results in an improved absolute upper limit for  $\hat{\alpha}$  of

$$|\hat{\alpha}| < 2.2 \times 10^{-7} \quad (7)$$

which is an improvement by one order of magnitude compared with the most accurate previous atomic beam measurements. This result is presently limited by the uncertainty of the rest frequency  $\nu_0$  [17], which enters (6) quadratically.

## 4. Outlook

Recently, several improvements have been made to the experiment. As already mentioned above, a higher laser switching frequency largely eliminates the influence of the laser forces on the Lamb-dip

frequency. Column 3 of Table 1 shows that this together with other improvements is expected to reduce the frequency uncertainty from 517 to 224 kHz.

However, to gain more sensitivity for  $\hat{\alpha}$ , a more accurate value for the rest-frame frequency is required. This can be deduced from a measurement on slow ions ( $\beta = 0.03$ ) at the TSR, which is currently under way. Column 4 of Table 1 summarizes the expected accuracy of this measurement. Taking both experiments together, we will be able to determine the rest-frame frequency  $\nu_0$  with an uncertainty of about 100 kHz and to improve the sensitivity on  $\hat{\alpha}$  by a factor of 3.

To further enhance the sensitivity to  $\hat{\alpha}$ , the ion velocity has to be considerably increased. At the experimental storage ring (ESR) of the Gesellschaft für Schwerionenforschung in Darmstadt,  $\text{Li}^+$  can be stored at velocities up to  $\beta = 0.45$ . When working, e.g., at  $\beta = 1/3$ , the Doppler shift leads to wavelengths of  $\lambda_p = 776$  nm and  $\lambda_a = \lambda_p/2 = 388$  nm, respectively, which can be generated by one laser and its 2nd harmonic. The frequency determination can be accomplished using a self-referenced frequency comb [18]. From an estimation of systematic errors based on the experience at the TSR, an improvement in the sensitivity to  $\hat{\alpha}$  into the  $10^{-9}$  range is expected.

The space-time symmetries of local Lorentz and CPT invariance are fundamental features of both the standard model of particle physics and general relativity. They are linked by the CPT theorem and by a recently proved reverse CPT theorem [19]. Violations of these symmetries are frequently discussed in the context of unification theories such as string theory [20] or loop quantum gravity [21]. While direct experimental signals caused by these models are expected on the Planck scale  $E_p \approx 10^{19}$  GeV, residual effects in high-precision low-energy experiments might be observable. One candidate signal for such effects is Lorentz violation. Preliminary results by Lane [22] indicate a unique sensitivity of Doppler-effect experiments to several parameters of the Standard Model extension of Colladay and Kostelecký [23], which provides a low-energy limit for Lorentz and CPT violating underlying theories. Moreover, their analysis shows that a modified version of our experiment exciting transitions between specific  $m$ -sublevels would constrain additional parameters of the model.

## Acknowledgements

We would like to thank U. Eisenbarth, M. Grieser, K. Horn, H. Krieger, S. Krohn, and R. Muñoz Horta for their help in the experiments. Helpful discussions with V.A. Kostelecký, C. Lämmerzahl, C. Lane, and M. Weidemüller are acknowledged.

## References

1. A. Einstein. *Ann. Phys.* **17**, 891 (1905).
2. H.P. Robertson. *Rev. Mod. Phys.* **21**, 378 (1949).
3. A.A. Michelson and E.W. Morley. *Am. J. Sci.* **34**, 333 (1887).
4. R.J. Kennedy and E.M. Thorndike. *Phys. Rev.* **42**, 400 (1932).
5. H.E. Ives and G.R. Stilwell. *J. Opt. Soc. Am.* **28**, 215 (1938).
6. A.A. Penzias and R.H. Wilson. *Astrophys. J.* **142**, 419 (1965).
7. R. Mansouri and R.U. Sexl. *Gen. Rel. Grav.* **8**, 497, 515, 809 (1977).
8. H. Müller, S. Herrmann, C. Braxmaier, S. Schiller, and A. Peters. *Phys. Rev. Lett.* **91**, 020401 (2003).
9. P. Wolf, S. Bize, A. Clairon, A.N. Luiten, G.Santarelli, and M.E. Tobar. *Phys. Rev. Lett.* **90**, 060402 (2003).
10. E. Riis, L.-U.A. Anderson, N. Bjerre, and O. Poulsen. *Phys. Rev. Lett.* **60**, 81 (1988).
11. D.C. Champaney, G.R. Isaak, and A.M. Khan. *Phys. Lett.* **7**, 241 (1963).
12. M. Kretschmar. *Z. Phys. A*, **342**, 463 (1992).
13. R.W. McGowan, D.M. Giltner, S.J. Sternberg, and S.A. Lee. *Phys. Rev. Lett.* **70**, 251 (1993).
14. D. Habs, W. Baumann, J. Berger et al. *Nucl. Instrum. Methods*, **B43**, 390 (1989).
15. R. Grieser, R. Klein, G. Huber et al. *Appl. Phys. B*, **59**, 127 (1994).
16. G. Saathoff, S. Karpuk, U. Eisenbarth et al. *Phys. Rev. Lett.* **91**, 190403 (2003).

17. E. Riis, A.G. Sinclair, O. Poulsen, G.W.F. Drake, W.R.C. Rowley, and A.P. Levick. *Phys. Rev. A*, **49**, 207 (1994).
18. T. Udem, R. Holzwarth, and T.W. Hänsch. *Nature*, **416**, 233 (2002).
19. O.W. Greenberg. *Phys. Rev. Lett.* **89**, 231602 (2002).
20. V.A. Kostelecký and S. Samuel. *Phys. Rev. D*, **39**, 683 (1989).
21. R. Gambini and J. Pullin. *Phys. Rev. D*, **59**, 124021 (1999).
22. C. Lane. *In Proceedings of the Third Meeting on CPT and Lorentz Symmetry. 4–7 August 2004. Bloomington, USA. Edited by V.A. Kostelecký. World Scientific, Singapore. 2005*
23. D. Colladay and V.A. Kostelecký. *Phys. Rev. D*, **58**, 116002 (1998).